Planetary and Space Science 246 (2024) 105905

Contents lists available at ScienceDirect

Planetary and Space Science

journal homepage: www.elsevier.com/locate/pss

Assessing the survival of carbonaceous chondrites impacting the lunar surface as a potential resource

Samuel H. Halim [a,b], Ian A. Crawford [a,b,*], Gareth S. Collins [c], Katherine H. Joy [d], Thomas M. Davison [c]

[a] Department of Earth and Planetary Sciences, Birkbeck, University of London, Malet St., London, WC1E 7HX, UK
[b] Centre for Planetary Sciences at UCL/Birkbeck, London, WC1E 6BT, UK
[c] Department of Earth Science & Engineering, Imperial College London, Kensington, London, SW7 2AZ, UK
[d] Department of Earth and Environmental Sciences, University of Manchester, Oxford Rd., Manchester, M13 9PL, UK

ARTICLE INFO

Keywords:
Moon
Space exploration
Impact processes
ISRU

ABSTRACT

The Moon offers a wide range of potential resources that may help sustain a future human presence, but it lacks indigenous carbon (C) and nitrogen (N). Fortunately, these elements will have been delivered to the Moon's surface by carbonaceous chondrite (CC) asteroid impactors. Here, we employ numerical modelling to assess the extent to which these materials may have sufficiently survived impact with the lunar surface to be viable sources of raw materials for future exploration. We modelled the impact of a 1 km diameter CC-like asteroid, considering impact velocities between 5 and 15 km s^{-1}, and impact angles between 15 and 60° to the horizontal. The most favourable conditions for the survival of C-rich, and especially N-rich materials, are those with the lowest impact velocities (≤10 km s^{-1}) and impact angles (≤15°). Impacts with velocities >10 km s^{-1} and angles >30° were found not to yield any significant amount of surviving solid material, where bulk survival is defined as material experiencing temperatures less than the impactor material's estimated melting temperature (~2100 K, based on a commonly adopted Equation of State for serpentine). Importantly, oblique and low velocity impacts result in concentrations of unmelted projectile material down-range from the impact site. For the canonical 1 km-diameter CC impactor considered here, with an impact angle ≤15° and velocity ≤10 km s^{-1}, this results in ~10^9–10^{10} kg of C and ~10^8–10^9 kg of N being deposited a few tens of km down-range from the impact crater, where it might be accessible as a potential resource. Such low-velocity and oblique impacts have a low probability - we estimate that only ~5 such impacts may have occurred on the Moon in the last 3 billion years (the number of impacts of smaller impactors will have been higher, but they will concentrate lower masses of potential resources). As the estimated C and N concentrations from such impacts greatly exceed those expected for ices within individual permanently shadowed polar craters, searching for these rare impact sites may be worthwhile from a resource perspective. We briefly discuss how this might be achieved by means of orbital infrared remote-sensing measurements.

1. Introduction

The surface of the Moon will be the next step in human space exploration, with an emphasis on developing approaches for *in situ* resource utilization (ISRU; e.g., ISECG, 2020). The Moon contains a wide range of raw materials that could support a human presence (for reviews see Anand et al., 2012; Crawford et al., 2023), but some key volatile substances, crucially including water, carbon, and nitrogen, are scarce on the lunar surface (McCubbin et al., 2023; Hurley et al., 2023). Mainly, this is a result of the Moon's different evolutionary history compared with the other terrestrial planets, especially its low gravity, lack of recent geological outgassing, and the consequent absence of geosphere-atmosphere-hydrosphere (and, for Earth, biosphere) interactions that lead to the processing and concentration of many biologically important materials. However, despite their scarcity, carbon (C) and nitrogen (N) will be important for supporting long-duration human missions to the lunar surface. For example, both elements will be required for lunar food production (e.g., Wamelink et al., 2014), with

* Corresponding author. Department of Earth and Planetary Sciences, Birkbeck, University of London, Malet St., London, WC1E 7HX, UK.
E-mail address: i.crawford@bbk.ac.uk (I.A. Crawford).

https://doi.org/10.1016/j.pss.2024.105905
Received 21 December 2023; Received in revised form 24 April 2024; Accepted 3 May 2024
Available online 4 May 2024

nitrogen also required as a buffer gas for an Earth-like breathable atmosphere. Carbon (combined with hydrogen) may also be important for carbo-thermal reduction of iron oxides to yield oxygen from lunar rocks (e.g. Prinetto et al., 2023), and for refuelling methalox-based spacecraft such as the SpaceX Starship (e.g., Cannon, 2021).

Fortunately, some of the desired volatile resources lacking in indigenous lunar materials are likely to have been delivered to the Moon from external sources. These include the solar wind (Fegley and Swindle, 1993), micrometeorites (e.g., Mortimer et al., 2016), and comet and asteroid impactors (e.g., Haskin et al., 1993; Wingo, 2004; Yue et al., 2013; Crawford et al., 2023). However, the concentrations of C and N in the lunar regolith due to solar wind and/or micrometeorite implantation are very low (~100 ppm; Fegley and Swindle, 1993) and it would require the processing of several cubic metres of regolith to extract one kg of these elements from that source (see Table 1 of Crawford, 2015). As discussed in Section 4 below, C and N are likely to be found in a more concentrated form in polar ice deposits (Colaprete et al., 2010; Cannon, 2021), but it would be of interest to determine if non-polar concentrations of these important elements are likely to occur on the Moon. In this context, it is interesting to note that C and N are abundant in carbonaceous chondrite (CC) meteorites sourced from asteroid parent bodies (e.g., Sephton, 2002; Pearson et al., 2006). Because asteroids with CC-like compositions will have impacted the lunar surface over geological time (e.g., Joy et al., 2012, 2016, 2020), these could be a useful source of these key elements on the Moon (a suggestion first made, to the authors' knowledge, in the science fiction novel *Worlds* by Haldeman, 1981). In this context, it is noteworthy that Yang et al. (2022) have identified what they interpret to be surviving metre-scale remnants of CC impactor material in multi-spectral images of the lunar surface obtained by the Yutu-2 rover at the Chang'e-4 landing site.

Unless, or until, significant quantities of surviving meteoritic materials are retrieved from the lunar surface, experimental and numerical modelling are the best tools to probe the fate of projectiles during and immediately after impact. Projectile survivability is influenced by multiple factors including impact velocity (Melosh, 1989; Bland et al., 2008; Kurosawa and Genda, 2018), projectile material properties (e.g., composition, density, strength, cohesion, etc; Daly and Schultz, 2013; Svetsov and Shuvalov, 2015; Wickham-Eade et al., 2018), projectile porosity (Wünnemann et al., 2008; Jutzi et al., 2008; Güldemeister et al., 2013), target porosity (Wünnemann et al., 2006; Avdellidou et al., 2016), target material properties (Christiansen et al., 1993; Davison et al., 2011; Burchell et al., 2014a), and angle of impact (Gault and Wedekind, 1978; Pierazzo and Melosh, 2000; Davison et al., 2011; Potter and Collins, 2013; Nishida et al., 2019). The survivability of rock projectile materials in numerically simulated hypervelocity impacts has been studied for multiple planetary bodies, including Earth (Pierazzo and Melosh, 2000; Wells et al., 2003; Potter and Collins, 2013; Beech et al., 2019), the Moon (Bland et al., 2008; Yue et al., 2013), asteroid 4 Vesta (Daly and Schultz, 2016); Europa (Pierazzo and Chyba, 2002), and Ceres (Bowling et al., 2020). In the case of the Moon, earlier numerical models have indicated that volatiles and organic material within projectiles may survive impact with the lunar surface (e.g., Crawford et al., 2008; Ong et al., 2010; Svetsov and Shuvalov, 2015). Projectiles in laboratory-scale experiments have been shown to survive hypervelocity impacts with a multitude of different target materials (e.g., Daly and Schultz, 2015; Wickham-Eade et al., 2018). Additionally, organic constituents within such projectiles have also been shown to survive (Mimura and Toyama, 2005; Parnell et al., 2010; Meyer et al., 2011; Burchell et al., 2014a, 2014b, 2017). Examples of surviving asteroidal material (see Joy et al., 2016) have been found in lunar samples from Apollo 11 (Goldstein et al., 1970), Apollo 12 (Wood et al., 1971; Zolensky et al., 1996; Joy et al., 2020), and Apollo 16 (Jolliff et al., 1993). Fragments of surviving meteoritic material have also been identified in lunar breccias, including a chondritic fragment within lunar meteorite Pecora Escarpment 02007 (Day et al., 2006; Liu et al., 2009; Joy et al., 2012), and younger Apollo 16 regolith breccias (Joy et al., 2012). From a resource perspective, it will be important to locate where surviving material may be concentrated in high enough abundances to be a useful resource (that is, to qualify as a 'reserve'; see Crawford et al., 2023). For example, if surviving meteoritic material is concentrated within a small area surrounding the impact site, it could become more attractive as an exploitable reserve. Although there have been previous investigations into the fragmentation of projectiles upon impact (e.g., Melosh et al., 1992; Nagaoka et al., 2013; Wickham-Eade, 2017; Nishida et al., 2019), there has been less work on the concentration of surviving fragments proximal to the impact site. Wieczorek et al. (2012) suggested that some lunar magnetic anomalies might be due to surviving fragments of metallic and/or ordinary chondrite impactors; Yue et al. (2013) suggested that projectile remnants may be concentrated in the central peaks of complex craters; and Potter and Collins (2013) investigated how large fragments of a meteorite have survived at the Morokweng crater on Earth. Further afield, Daly and Schultz (2016) suggested that craters on Vesta may preserve localised deposits of carbonaceous projectile material.

If meteoritic material survives impact with the lunar surface, it will gradually be degraded by micrometeorite impacts and other surface processes. The median survival time for centimetre to meter scale rocky material on the surface of an airless body like the Moon has been estimated to be between 40 and 80 Ma, with some surviving up to 300 Ma, depending on the material (Basilevsky et al., 2013, 2015). This means that for impacted projectile material to survive over long periods of time (i.e., millions or billions of years) after impact, the material must be protected from destructive processes at the surface. Rapid burial by crater and basin ejecta, and/or by mare basalt flows, could potentially provide protection for meteoritic material (e.g., Crawford and Joy, 2014; Joy et al., 2016), but to be useful as a resource it would need to be

Table 1
Abundances of C-bearing materials found in a range of CM/CI meteorites (Murchison, Murray and Orgueil) and the average abundances of N-bearing molecules found in CM meteorites (Murchison and Murray) and associated vaporisation temperatures included for both C- and N-bearing molecules (we have assumed that these compounds are homogeneously distributed within the meteorites).

Carbon type	Abundance (wt.%)[1],[2],[3]	Vaporisation temperature (K)	Nitrogen type	Abundance (ppm)[6]	Vaporisation temperature (K)[7]
Organic matter	0.6–2.3	550–750[1]	Glycine	4.5	525
Carbonate	~0.2	700–1000[1]	Glutamic acid	2.3	700
Diamond	0.03–0.15	4000[4]	Aspartic acid	1.7	600
Graphite	0.001–0.005	4000[4]	Glutamine	1.1	850
Silicon carbide	0.001–0.009	3000[5]			

[1] Huss and Lewis (1994).
[2] Russell et al. (1996).
[3] Sephton (2002).
[4] Bundy (1989).
[5] NIOSH (2019).
[6] Cronin & Moore (1971).
[7] Weiss et al. (2018).

Table 2
Equations of state (EoS) available within the iSALE EoS library which were considered to represent carbonaceous chondrite (CC)-like material.

Equation of state	Previous use in modelling work
Granite – ANEOS (Pierazzo et al., 1997)	Multiple studies have used both in a variety of lunar impact simulations, but less so as CC-like material. (e.g., Crawford et al., 2008;
Basalt – ANEOS (Pierazzo et al., 2005)	Potter, 2012; Kring et al., 2016). Used here for comparison vs. more likely candidate materials.
Quartz – ANEOS (Melosh, 2007)	Approximation for hydrated asteroid material impacting the Moon (Svetsov and Shuvalov, 2015).
Dunite – ANEOS (Benz et al., 1989)	Simulation of CM-like impactor striking Vesta (Turrini et al., 2014).
Serpentine – ANEOS (Brookshaw, 1998)	Hydrocode modelling as the surface of a CC-like asteroid (Richardson et al., 2005) and as the hydrated core of planetesimal impacts (Wakita and Genda, 2019).
Carbchon – Tillotson (Herbold et al., 2015)	Specifically created by Herbold et al. (2015) to represent CI/CM material.

exhumed, either naturally via impact gardening or, in the more distant future, by mining activities.

In this paper, we report hydrocode modelling of the impact of a 1 km diameter CC-like asteroid into a simulated basaltic lunar surface to assess the distribution of surviving impactor fragments, and the extent to which C- and N-rich materials contained within them may survive impact sufficiently to be viable sources of raw materials for future human exploration activities. We also briefly consider how such material might be located on the lunar surface.

2. Methods

Investigation of both the temperature regimes and the location of CC material post-impact requires a suite of 3D impact models at a variety of impact angles and velocities. Here, we have made use of the iSALE (impact-SALE) multi-material, multi-rheology shock physics code (Wünnemann et al., 2006); iSALE is itself based on the SALE (Simplified Arbitrary Lagrangian Eulerian) hydrocode (Amsden et al., 1980). Hypervelocity impact processes are simulated in solid materials and can include an elasto-plastic constitutive model, fragmentation models, various equations of state, and multiple materials (Melosh et al., 1992; Ivanov et al., 1997); more recent developments of the model have been described by Collins (2014), Collins et al. (2011a, 2014), and Wünnemann et al. (2006). iSALE has been benchmarked against other hydrocodes (Pierazzo et al., 2008) and validated against experimental data from laboratory scale impacts (e.g., Pierazzo et al., 2008; Davison et al., 2011; Miljković et al., 2012), and is able to simulate impact processes in both two- and three-dimensional space. The 3D version (Elbeshausen et al., 2009) includes a fast and accurate adaptive interface reconstruction algorithm (Elbeshausen and Wünnemann, 2011) and is parallelised by using Message Passing Interfaces (MPI). In this work, high spatial resolution 2D simulations were used to determine accurate temperature and pressure regimes across the projectiles via a resolution test; 3D simulations are more limited in terms of resolution compared to 2D (due to computational requirements), but they allow us to predict the location of the projectile material following oblique impacts.

Owing to our focus on possible resource utilization, we have considered CI and CM carbonaceous chondrite compositions for the impactor material, as these contain the highest proportion of C and N within meteorite samples investigated so far (e.g., Alexander et al., 1998; Sephton, 2002; Pearson et al., 2006). Typical concentrations of some C- and N-bearing compounds in these meteorites are presented in Table 1 (see the footnotes for references to specific meteorites). We represent the impactor using a material model best approximating CC-like material from those available in the iSALE library. Based on previous modelling work involving CCs, and consideration of materials which represent the best approximation of the bulk composition of CC materials, a set of Equations of State (EoS) were tested (Table 2). The Carbchon Tillotson EoS aims to represent solid CI/CM material, but is not included in the iSALE EoS library and was added from Herbold et al. (2015). The other five materials use a semi-analytical equation of state (ANEOS; Thompson and Lauson, 1972). Fig. 1 shows the response of the materials to shock for a solid projectile impacting a solid target, using combinations of shock pressure, particle velocity, and shockwave velocity (available within the iSALE EoS library). These data were compared with experimental shock Hugoniot data for the composition of CM2 (Murchison) and ordinary L-type (Bruderheim) chondrites (Anderson and Ahrens, 1998). Dunite behaves more like ordinary chondrites than CC material, plotting near or above that of the Bruderheim data and far from the Murchison data. Similarly, basalt plots further from the CM2 data than other candidate materials. Therefore, dunite and basalt can be discounted as potential representations of CC material. Quartz, serpentine, granite, and carbchon all plot in very similar positions in both Fig. 1a and b.

With the introduction of a porosity model simulating 20% of the volume as pore space (based on the porosity for a typical CC meteorite; e.g., Consolmagno et al., 2008), both serpentine and the CC Tillotson EoS match well to the Murchison material data (Fig. 2). Based upon this investigation of potential projectile materials, serpentine was chosen as the material to be used for the 2D and 3D iSALE simulations reported here. Choosing this material model over the similarly performing CC Tillotson EoS, despite the latter being specifically created to represent CM material, was based on several factors: the serpentine ANEOS has been used in previous simulations representing carbonaceous material (Richardson et al., 2005; Davison et al., 2016; Wakita and Genda, 2019), and ANEOS enables estimation of phase changes within materials, which is important in the context of CC survival and its resource potential.

High spatial resolution 2D simulations were used to determine temperature and pressure regimes across the projectile via a spatial resolution test. In impact simulations, spatial resolution is typically expressed as the number of cells per projectile radius (CPPR). We simulated each scenario at resolutions of 8, 16, 24, 32, 50, 100, and 200 cells per projectile radius and measured the volume of the projectile that experiences peak temperatures higher than the melt temperature of the serpentine projectile material (~2100 K; Brookshaw, 1998).[1] Using iSALE-2D (Wünnemann et al., 2006), we modelled the vertical impact of a 1-km diameter, CC-like projectile into a single-layer, lunar surface target at 5 km s^{-1}. Thermal, strength and damage parameters were adopted as appropriate for a CC projectile and the lunar crust (see table 6.2 of Halim, 2023). A serpentine ANEOS EoS (Brookshaw, 1998) was used for the projectile, with an assumed (macro) porosity of 40% based on average values for CC asteroid parent bodies (Veverka et al., 1999; Britt et al., 2002; Chesley et al., 2014; Lauretta et al., 2015; Sugita et al., 2019). The material model used to represent the target combined an ANEOS-derived EoS table for basalt (Pierazzo et al., 2005) with 10% porosity modelled using the epsilon-alpha compaction model (Wünnemann et al., 2006; Collins et al., 2011a). A target porosity of 10% was adopted as an approximate average for the lunar highlands

[1] We recognize that melts may also be produced at lower temperatures during the shock release stage (we are grateful to a referee for pointing this out). However, we are doubtful that this will greatly affect the survival of C- and N-rich compounds as potential resources because C and N-rich compounds within these melts are likely to remain trapped within the projectile remnants when the material re-solidifies (see discussion in Section 3). Note also that most of the material of interest in a resource context (Fig. 5a and b) has been subjected to maximum peak-shock temperatures of $\leq$1000 K which are well below the melting temperature; assessing the degree of pressure release melting at these low temperatures would require a further study.

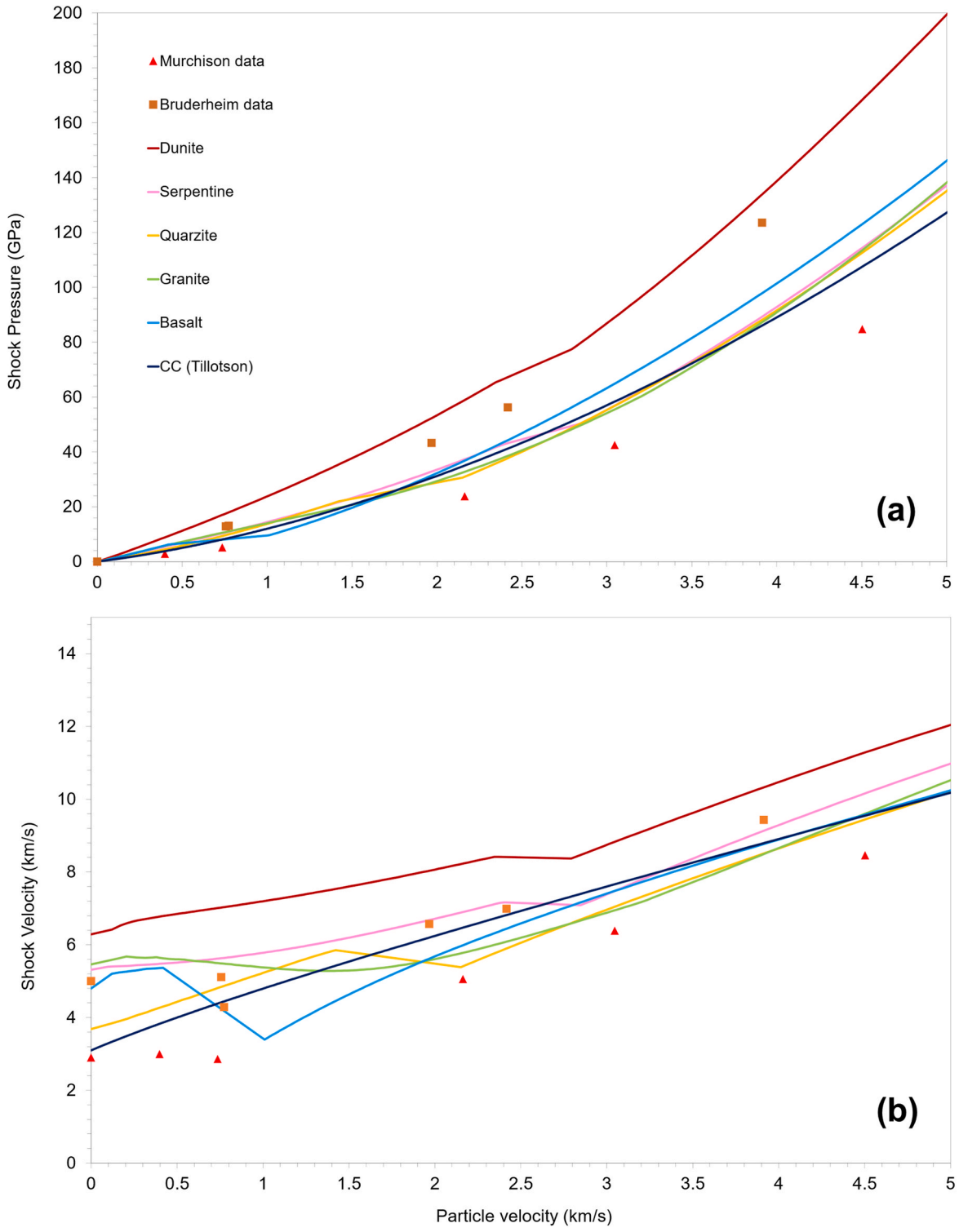

Fig. 1. A comparison of shock Hugoniot data for iSALE EoS data (dunite, serpentine, quartzite, granite, basalt, and CM carbonaceous chondrites (CC) material models) and experimental data for ordinary L chondrites (Bruderheim) and CM carbonaceous chondrites (Murchison). Bruderheim and Murchison data taken from Anderson and Ahrens (1998). (a) Particle velocity vs. shock pressure, (b) particle velocity vs. shock velocity.

megaregolith (Wieczorek et al., 2013), although we note that the porosity of the uppermost few km might be higher in places depending on the local structure of the megaregolith (determining the effects of which would require additional modelling). Although basalt is not the most appropriate compositional analogue for lunar highlands material, this material model was favoured as no ANEOS-derived table for anorthosite is currently available. Previous work has shown that impactor survivability depends most sensitively on the shock response of the impactor and target materials (e.g., Potter and Collins, 2013). As the density (2860 *vs* 2940 kg m^{-3}), bulk sound speed (5 *vs* 4.9 km s^{-1}) and the slope of the linear shock-particle speed relationship (1.62 *vs* 1.53) are similar for basalt and gabbroic anorthosite (O'Keefe and Ahrens,

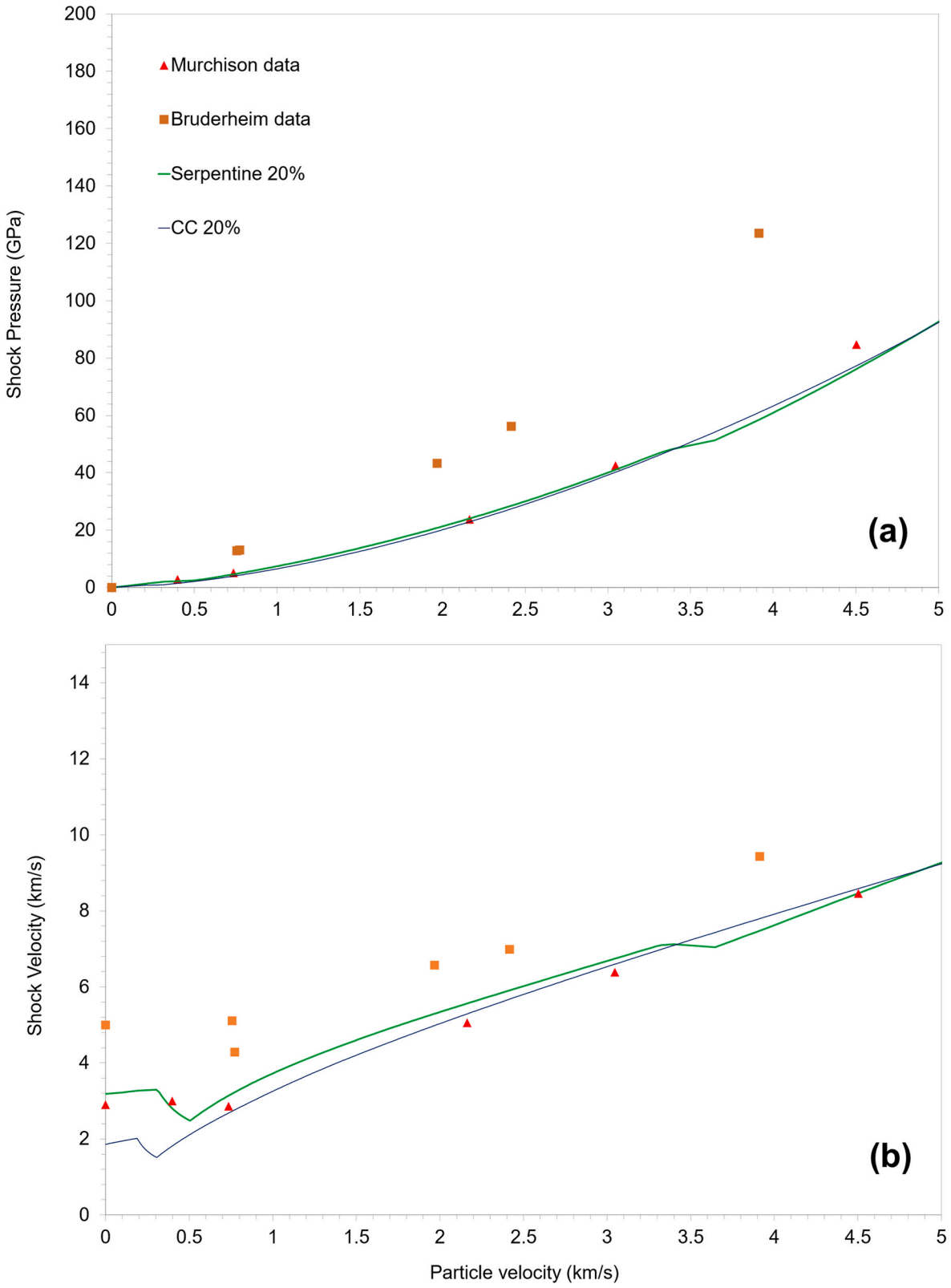

Fig. 2. A comparison of shock Hugoniot data for iSALE EoS (serpentine and carbonaceous chondrites (CC), both including 20% porosity) and experimental data for ordinary L chondrites (Bruderheim) and CM carbonaceous chondrites (Murchison). Bruderheim and Murchison data taken from Anderson and Ahrens (1998). (a) Particle velocity vs. shock pressure, (b) particle velocity vs. shock velocity.

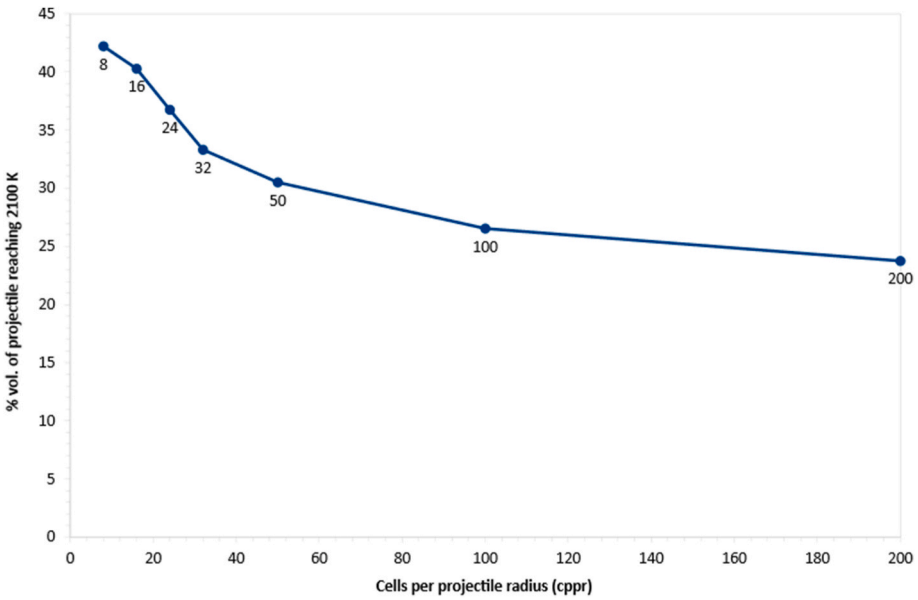

Fig. 3. Resolution study for the 2D, vertical impact described in the text, showing the volume (%) of the projectile which reaches a certain temperature (y-axis) at increasing amounts of cells per projectile radius (CPPR).

1982), we do not expect our conclusions to be sensitive to our choice of target material model.

Fig. 3 shows the results of this resolution test, with the volume of material experiencing temperatures greater than that of the melt temperature decreasing with increasing resolution. At the highest resolution tested (200 cells per projectile radius) the results are close to converged, and it is likely that the volume of material reaching the melt temperature would only decrease slightly more for higher resolution simulations. Based on this 2D resolution test, and previous work that showed very similar sensitivity to resolution of heated volumes between iSALE2D and iSALE3D (Davison et al., 2014), we conservatively assume that the temperatures recorded in the lower resolution 3D simulations will be overestimated compared to what they would be in a "real-world scenario" (converged with an essentially infinitely high resolution). For example, a simulation run at 16 cells per projectile radius would overestimate the volume of the projectile that reached a given temperature by ~70% when compared to an identical simulation at 200 cells per projectile radius. The 3D simulations were carried out on the Kathleen High-Performance Computing (HPC) Facility at University College London (Kathleen@UCL). A resolution of 16 cells per projectile radius was chosen as a compromise between relatively accurate calculation of temperatures in the projectile and the computational time taken to run long enough to record where the projectile material lands after impact. The compositions, porosities and EoS for the projectile and target were the same as adopted for the 2D simulations. Although the average impact velocity for asteroidal bodies striking the Moon has been estimated to be between ~14 and 20 km s^{-1} (e.g., Ivanov, 2001; Marchi et al., 2009; Le Feuvre and Wieczorek, 2011), from a projectile survival perspective we are mostly interested in below average impact velocities and have here modelled impact velocities of 5, 10, and 15 km s^{-1}, with impact angles ranging between 15 and 60° to the horizontal (Table 3). Fig. 4 shows snapshots of the cratering process for the 5 km s^{-1} 15° impact scenario, which is the most relevant from a resource perspective (discussed below).

Table 3
Names assigned to each of the 12 different scenarios covered by this suite of simulations by varying impact velocity and angle.

Angle (°)	Velocity (kms^{-1})		
	5	10	15
15	a15_v5	a15_v10	a15_v15
30	a30_v5	a30_v10	a30_v15
45	a45_v5	a45_v10	a45_v15
60	a60_v5	a60_v10	a60_v15

Lagrangian tracer particles were placed in each cell of the projectile to track temperature, pressure, and the location of the material over the course of the impact. A gravitational acceleration of 1.62 ms^{-2} was applied across the scenarios, consistent with that of the lunar surface. The simulations were run for 48 h on the Kathleen HPC, corresponding to a maximum simulated time of 25 s after impact. For the shallow impacts where projectile 'decapitation' occurs (Davison et al., 2011; see below), most of the least shocked projectile material comes to rest within the iSALE simulation. However, high-velocity projectile material was found to still be travelling away from the impact site after this time (see Fig. 4), and this was ballistically projected to a final resting place on the lunar surface. This was achieved by identifying the launch position and ejection velocity vector of each projectile tracer at some point before the end of the simulation and then calculating its ballistic trajectory to predict its final landing location. However, as different parts of the projectile begin ballistic motion at different times, it is difficult to define a simple protocol for the moment of launch. The solution adopted in this work included ballistic calculations for different parts of the simulation (an example script can be found in Appendix A6 of Halim, 2023). Firstly, any projectile material with an upward motion above the elevation of the pre-impact surface (z = 0; see Fig. 4) was projected forward, using tracer particles to track when material was ejected and the three components of their velocity to calculate a final landing location on the lunar surface. Secondly, any projectile material originating from within the transient crater, below the pre-impact surface, that experienced an upward motion by the end of the simulation was projected from the last point at which its velocity was defined. Due to the location of these tracers within the growing transient cavity, these tracers may not have been moving ballistically at the time of projection, so this simplification may lead to uncertainties in the final landing locations. Thirdly, some tracers were found downrange of the transient crater that had never experienced an upward motion and were located beneath the pre-impact surface by the end of the simulation (especially in the 15° impacts); this is interpreted as projectile material that scours the lunar surface and its final resting place was assumed to be on (or just below) the surface. Finally, any material that achieved a velocity greater than the escape

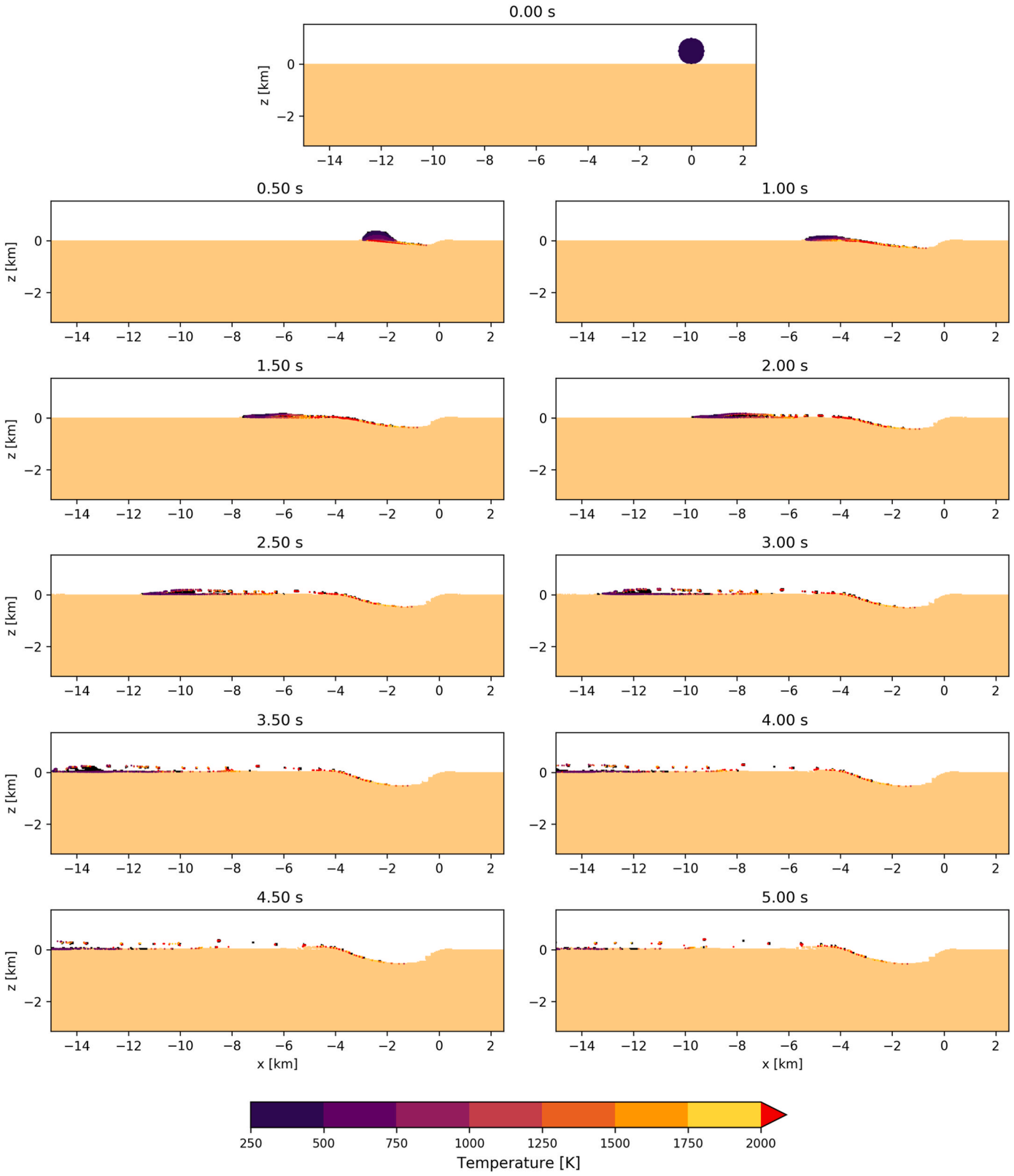

Fig. 4. Snapshots of the first 5 s of the impact process in the y = 0 plane for a 1 km diameter projectile striking the lunar surface at 5 km s^{-1} with an angle of 15° to the horizontal (i.e., scenario a15_v5). The decapitated projectile skids across the surface downrange of the crater, scouring the surface and shedding low shock surviving fragments. Black denotes projectile material in the computational grid; the temperature scale records the peak temperatures experienced by the projectile tracer particles.

velocity of the Moon (2.38 km s^{-1}) whilst experiencing an upward trajectory was removed from the calculations.

3. Results

We take the theoretical melting temperature of the projectile material (~2100 K; Brookshaw, 1998) to provide a conservative estimate for the survival of solid projectile material in the impact ejecta. Table 4 shows the percentage of the projectile mass that remains solid after impact according to this criterion. For a low impact velocity (5 km s^{-1}), the majority of projectile material remains solid for all impact angles considered. Similarly, the lowest angle impacts considered (15°) allow for solid material survival at all impact velocities up to 15 km s^{-1}. However, impacts with velocities >10 km s^{-1} and angles >30° do not yield any surviving solid material and so are not relevant as prospective resources.

The relative proportion of surviving projectile material that (i) remains within the crater, (ii) is ejected beyond the crater rim, and (iii) escapes from the Moon is shown in Table 5. The proportion of material found within the transient crater by the end of the impact increases with increasing impact angle. In the scenario with the lowest impact angle (15°) and velocity (5 km s^{-1}), the vast majority (96%) of the projectile volume lands on the target surface outside the crater, with 4% escaping. Increasing impact velocity for this oblique impact angle leads to a significant increase in the amount of material expected to escape the lunar gravity, rising to 48% at 10 km s^{-1} and 71% at 15 km s^{-1}, reducing the mass remaining as a potential resource (although some ejected material may re-impact into the Moon at a later time, it is impossible to say where that material would be found).

Figs. 5 and 6 show the final resting locations of surviving solid projectile material on the lunar surface (plan view), colour coded according to maximum peak temperature experienced during the impact. Based on the vaporisation temperatures shown in Table 1, we would expect the hardiest C-bearing compounds (i.e., SiC, diamond, graphite) to remain *in situ* in the projectile remnants at all the locations plotted, but more volatile compounds are likely to be lost (at least partially). A conservative estimate of the extent to which these compounds may remain within surviving projectile fragments can be obtained by comparing the vaporisation temperatures listed in Table 1 with the peak impact temperatures shown in Figs. 5 and 6. Such a comparison will be conservative for two reasons: (i) the peak temperature reached within any projectile cell typically lasts for less than one timestep (0.5 s), and it may be doubted that all the affected molecules vaporise and escape from the surrounding (solid) projectile matrix in this short time; and (ii) some fraction of vaporised material will likely recondense locally within the projectile fragments before escaping, and hence remain available as a potential resource.

As would be expected, the best scenario for the preservation of C- and N-bearing materials is the lowest velocity and most oblique impact considered (e.g., scenario a15_v5; Figs. 4 and 5a). Approximately 85% of the projectile remains solid (Table 4), and ~16% of the original projectile mass experiences temperatures less than 700 K suitable for the survival of most of the carbon species and many of the organic materials (including the nitrogen-containing amino acids; we recognize that amino acids may undergo thermal decomposition into constituent atoms and molecules at temperatures lower than the vaporisation temperatures listed in Table 1, but if the surrounding bulk material remains solid it seems likely that the decomposition products will remain trapped in the surviving projectile fragments). Importantly, for this scenario, the majority of the surviving material suitable for the survival C- and N-bearing molecules (<700 K, dark purple in Fig. 5a) is found concentrated in a small area extending from ~20 km to ~30 km downrange and is spread over an area of ~60 km^2. This concentration of less shocked projectile material downrange of the impact site results from the phenomenon of 'projectile decapitation' (Davison et al., 2011), whereby some of the trailing part of the projectile, which suffers the least shock on impact, separates from the remainder and travels further downrange with reduced velocity, This effect can be seen in Fig. 4, and is discussed in Chapter 6 of Halim (2023; see his figures 6.1 and 6.7). The decapitated projectile skids along the surface and parts of the low-shock trailing edge (tracked by Lagrangian tracer particles) scour and become entrained in the uppermost target material. While the state of the projectile fragments, as well as the extent of entrainment and depth of mixing is under resolved in our simulations, the surviving projectile fragments and their volatile compounds are expected to come to rest close (i.e. ≤10 m depth) to the surface.

Fig. 5b shows the results for scenario a15_v10, where the increased velocity has decreased the amount of surviving material subjected to low temperatures, with 58% of the projectile remaining solid (Table 4). A minimum temperature of 800 K is experienced by all of the projectile, with just ~3% of the original projectile volume experiencing temperatures <1000 K. These temperatures would potentially enable the survival of some carbonate species, and some amino acids (e.g., glutamine), according to the vaporisation temperatures listed in Table 1; the more durable C-bearing molecules will likely remain in the majority of the surviving projectile. The bulk of the surviving material is again found within a decapitation zone downrange of the impact, which is now closer to impact site.

Increasing the impact velocity further to 15 km s^{-1} (a15_v15; Fig. 5c) results in minimum temperatures of ~1400 K and just ~21% of the projectile volume remaining solid after impact (Table 4). All of the amino acids considered would be vaporised in this scenario and the only C-bearing molecules to survive in significant quantities would be the most durable (i.e., SiC, graphite, and diamond). This material is again concentrated as a cone shape extending from the point of impact to ~30 km downrange, becoming sparser with distance from the impact.

Less oblique impact angles lead to higher peak temperatures across a greater proportion of the projectile volume but concentrate more of the surviving projectile material closer to the crater (Fig. 6). At 30° (Fig. 6a), almost three-quarters of the projectile remains solid (Table 4), but only a small (~1%) volume of the projectile records temperatures <1000 K. As would be expected, at higher impact angles the surviving projectile fragments become increasingly concentrated around the crater, but are subject to higher temperatures, making them even less attractive as possible sites for C- and N-rich resources. Note that the concentric

Table 4
Percentage of CC projectile material (assumed macro-porosity of 40%) that remains solid after impact, based upon peak temperatures reached within the projectile at any time during the simulation.

Angle (°)	Velocity (kms^{-1})		
	5	10	15
15	85%	58%	21%
30	74%	0%	0%
45	65%	0%	0%
60	57%	0%	0%

Table 5
Proportions of projectile volume in their respective final locations after impact for scenarios where solid material survived. Results are rounded to the nearest percent, apart from proportions <0.5% to avoid misrepresentation of a small amount of material that does in fact remain within the craters formed.

Scenario	Proportion of projectile material in final location		
	Landed in crater	Landed ejecta	Escaped
a15_v5	<0.5%	96%	4%
a15_v10	<0.5%	52%	48%
a15_v15	<0.5%	29%	71%
a30_v5	9%	47%	44%
a45_v5	34%	56%	10%
a60_v5	51%	48%	1%

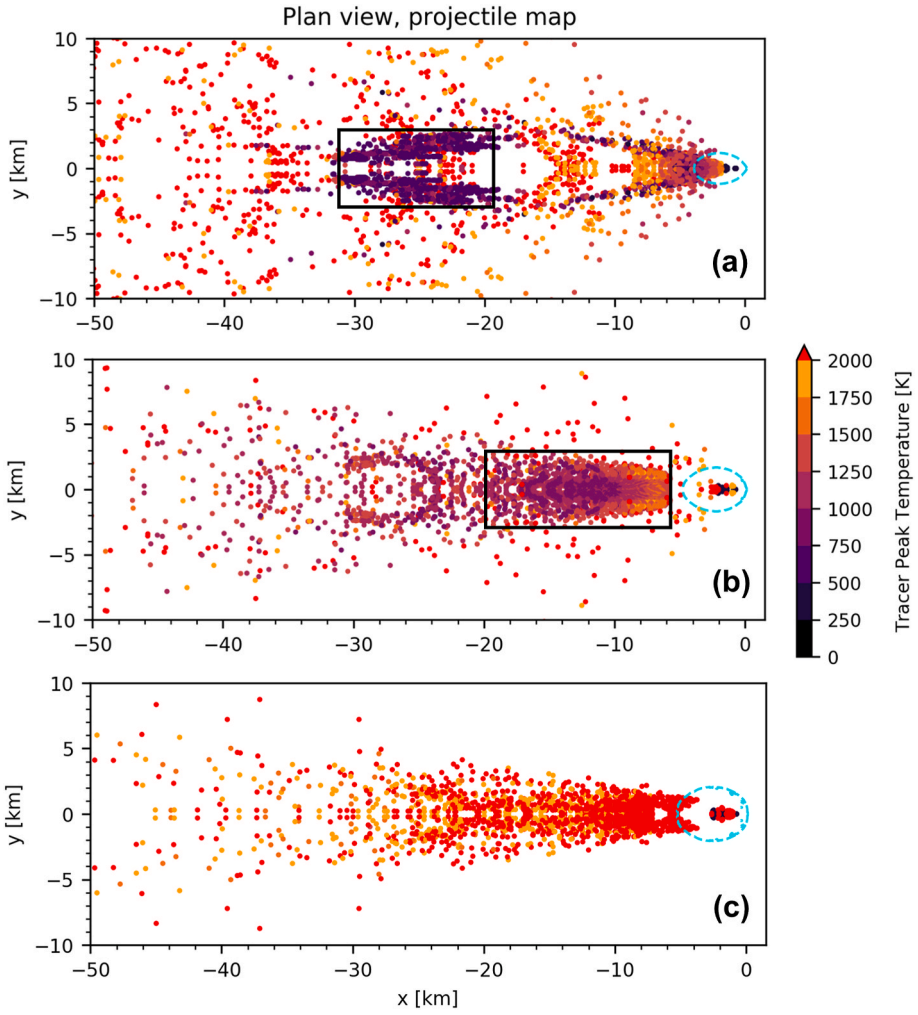

Fig. 5. Peak temperature and location plots of the fate of a 1 km diameter projectile following impact on the lunar surface in scenarios (a) a15_v5, (b) a15_v10, and (c) a15_v15. Each tracer represents a cube of projectile material with initial dimensions 31.25 × 31.25 × 31.25 m. Light blue (cyan) coloured dashed line shows the approximate location of the transient crater rim. Direction of impact is from right to left, with the initial impact point located at [0,0]. Black boxes in (a) and (b) highlight the areas where surviving CC projectile material is expected to be concentrated.

banding of final projectile locations apparent in Fig. 6b and c is an artefact of the ballistic projections resulting from the 0.5s timesteps of the model; in reality, some of the material plotted within these bands will be distributed into the spaces between them, resulting in lower surface concentrations at distal locations than implied by these figures.

4. Discussion

4.1. Surviving masses of resource-rich material

We can estimate the masses of surviving C- and N-rich material available as potential resources by (i) converting the fractional mass within each cell exposed to temperatures below each compound's vaporisation temperature (Table 1); and (ii) converting to kg based on the initial mass of the projectile and the assumed abundances of C- and N-rich compounds within it. These mass calculations are based on the mass of the 40% porous, 1 km diameter, serpentine material impactor, with a total impacting mass of ~7.6×10^{11} kg.

As discussed above, the most favourable case for the survival of resource-rich materials is lowest velocity (5 km s^{-1}), lowest angle (15°) impact considered (i.e., model a15_v5; Fig. 5a) as this is the only one where significant N-bearing compounds are not heated to above their vaporisation temperatures. The least shocked projectile material will be found within the 'decapitation zone' (purple points bounded by a black rectangle in Fig. 5a), approximately 20–30 km downrange of the impact site. Fig. 7a depicts the maximum temperatures reached within the total mass of surviving material in this decapitation zone. Approximately 3×10^{10} kg of material in this zone experiences maximum temperatures permitting the survival of glutamic acid (<700 K), with up to 7×10^{10} kg experiencing temperatures suitable for glutamine (<850 K). Organic carbon, the form of carbon with the highest wt.% in CCs (Table 1) is likely to survive in ~5×10^{10} kg of the decapitated projectile, with temperatures suitable for carbonate survival in ~8×10^{10} kg. Factoring in the abundances of the various C- and N-bearing compounds within known meteorite classes (Table 1), we estimate that the decapitation zone of 1 km-diameter CI asteroid impacting at 5 km s^{-1} and 15° to the horizontal would be expected to contain ~5.7×10^9 kg of C and ~5.7×10^8 kg of N; the corresponding values for a CM impactor are ~2.6×10^9 kg and ~1.1×10^8 kg, respectively (the breakdown for specific compounds can be found in table 6.7 of Halim, 2023).

Fig. 7b shows the results for a comparable analysis for the next most favourable case (i.e., model a15_v10; Fig. 5b). Here, the total mass of projectile debris surviving in the decapitation zone is about twice as much as for the a15_v5 case, but both the fractional and absolute masses of non-volatilised C- and N-bearing compounds is lower owing to the higher peak shock temperatures. Still, if a substantial fraction of C and N were to remain trapped within the solid projectile fragments, despite transient heating to above their vaporisation temperatures, then our

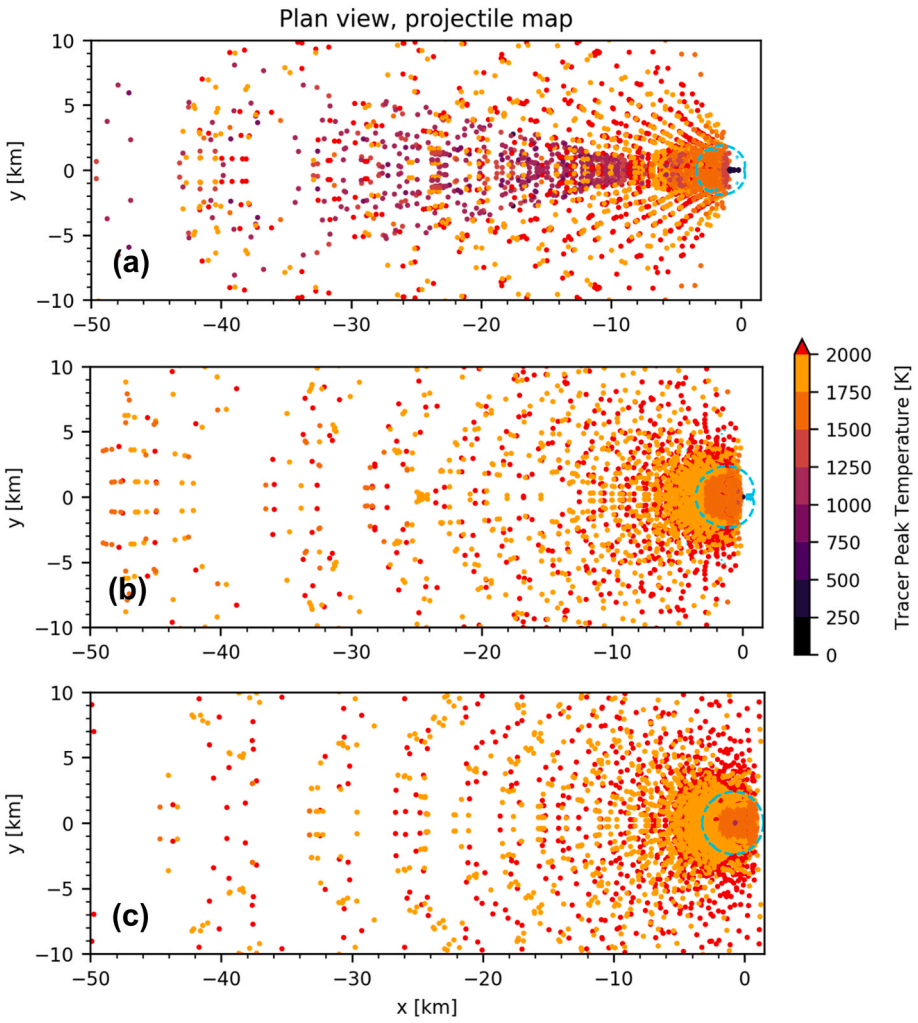

Fig. 6. As for Fig. 5 for scenarios (a) a30_v5, (b) a45_v5, and (c) a60_v5. The concentric nature of the modelled ejecta deposition is an artefact owing to limitations in the temporal and spatial resolution of the simulations (see text).

models predict ~1.2×10^{10} kg of C and ~1.2×10^{9} kg of N for the same 1-km diameter CI impactor; the corresponding values for a CM impactor are ~5.5×10^{9} kg and ~2.3×10^{8} kg, respectively.

It is interesting to compare the predicted C abundances with those inferred for ices preserved in permanently shadowed regions (PSRs) at the lunar poles (Cannon, 2021). Brown et al. (2022) have estimated the masses of water ice in several PSRs and obtain values in the range 10^{7}–10^{10} kg. Applying Cannon's (2021) estimate that lunar ices probably contain ~6% C (mostly in the form of molecules such as CO, C_2H_4, CO_2, CH_3OH, and CH_4), we estimate that a typical lunar PSR might contain ~6×10^{5} to 6×10^{8} kg of C. Given that the LCROSS impact results (Colaprete et al., 2010) found that NH_3 in PSRs also has an abundance of ~6% of the water abundance, we would expect similar masses of N in a typical PSR. Thus, the debris surviving from a single large (~1 km diameter) CC asteroid with the Moon could potentially provide over an order of magnitude more C, and up to an order of magnitude more N, than a typical PSR. Moreover, the PSR deposits would likely be spread over areas of several hundred square km (Brown et al., 2022), whereas surviving debris from a CC impactor will be significantly more concentrated (i.e. within a few tens of km^2 in the 'decapitation zone' of an oblique impact). Therefore, the remains of low velocity, oblique CC impactors may provide the most concentrated form of these important elements at the Moon's surface.

4.2. Probability estimates for oblique, low velocity CC impacts into the moon

Having determined that the best locations for finding a high proportion of surviving C- and N-rich projectile fragments will be the decapitation zone downrange of low velocity (~5–10 km s^{-1}), low angle (~15°) impacts (Fig. 5a and b), we need to assess how many such impacts are likely to have occurred on the Moon throughout its history. The probability (P_r) of a projectile impact into a target surface at an angle $<\theta$ (measured from the surface) can be determined via the empirical and theoretically well-established equation (Michikami et al., 2017, adapted from Elbeshausen et al., 2013; Shoemaker, 1962):

$$P_r = 0.5(1 - \cos(2\theta))$$

Using this equation, we can determine that the probability of an oblique impact for any projectile at $\leq 15°$ is ~6.7%.

We also need to determine the probability of such an oblique impact occurring at a sufficiently low velocity. Unfortunately, from a resource survival perspective, the probability of low-velocity impacts on the Moon is very low. Based on the present-day configuration of the Solar System (which is probably representative of the last 3 billion years), Marchi et al. (2009) find that only ~1% of all impactors will strike the Moon with velocities ≤ 5 km s^{-1}, and that ~17% impact with velocities ≤ 10 km s^{-1}.

Combining this with the assumption that about one third of all lunar

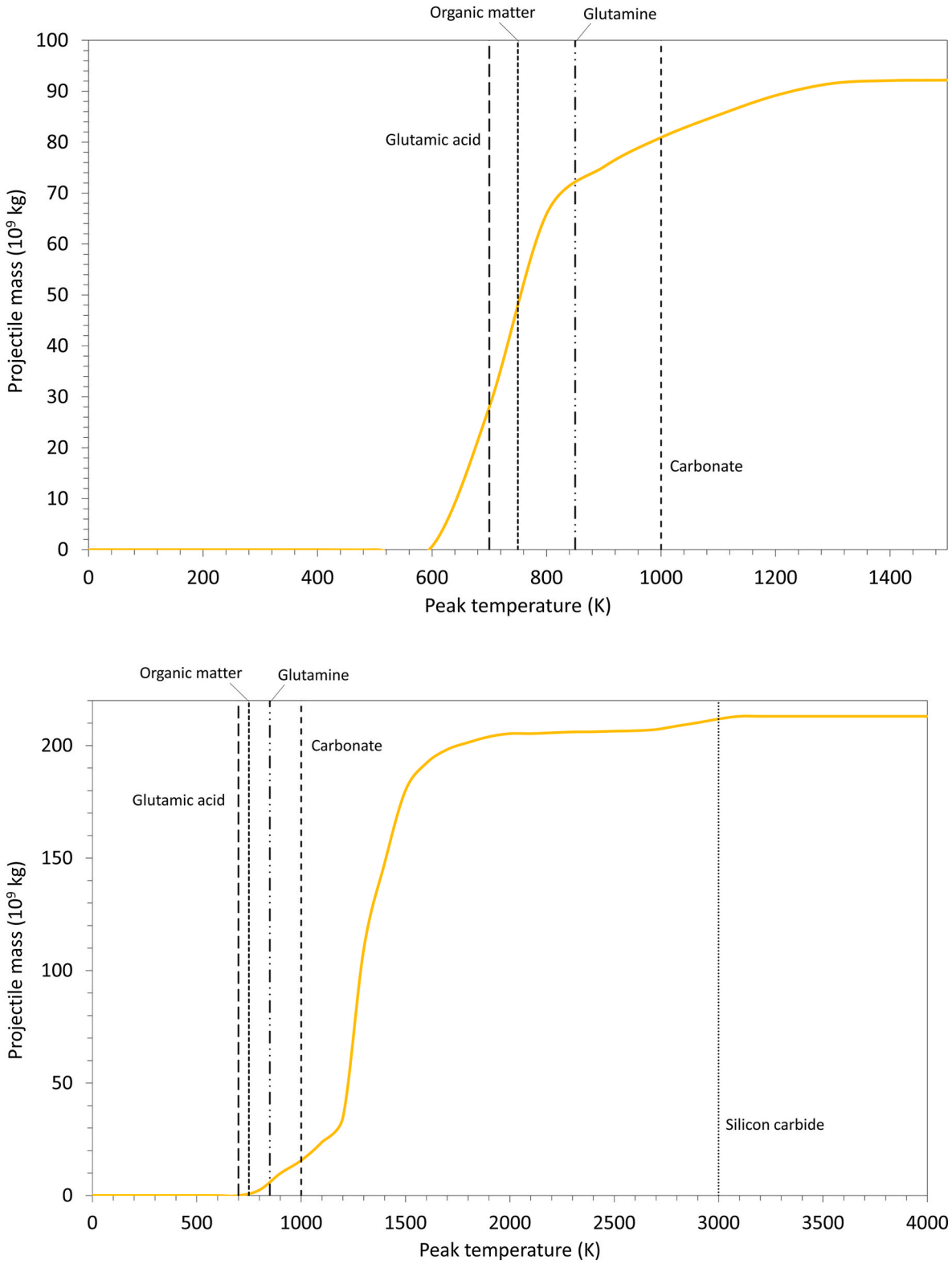

Fig. 7. (a) Cumulative mass of the decapitated portion of the projectile highlighted in Fig. 5 (simulation a15_v5) as a function of peak temperature experienced during the impact event; vaporisation temperature thresholds from Table 3 are plotted as dashed lines. **(b)** As for (a) but for the a15_v10 simulation; note that a smaller fraction of the surviving mass experiences peak temperatures below the vaporisation temperatures of key C- and N-bearing compounds than in (a) but that the total mass of unmelted projectile material in the decapitation zone is higher.

impacts are produced by C-type asteroids (Shoemaker et al., 1990), the fraction of lunar impacts similar to scenarios a15_v5 and a15_v10 (Fig. 5a and b) is $\sim 2 \times 10^{-4}$ and 4×10^{-3}, respectively. Using the model cumulative size distributions of the number of impactors on the Moon with diameters $\geq$1 km (1×10^{-14} km^{-2} yr^{-1}; Marchi et al., 2009), and the surface area of the Moon (3.794×10^{7} km^2), we would predict ~5

impacts with the combination of a CC asteroid with a diameter >1 km, an impact angle <15°, and a velocity <10 km s^{-1} over the past ~3 billion years. Identifying such a small number of CC-rich impact sites will be challenging (see Section 4.3 below), but, given that their resource potential compares favourably with polar PSRs, doing so may still be worthwhile. In any case, this number should be viewed as a minimum estimation for impacting bodies of a relatively large size (>1 km diameter) because impact rates earlier in Solar System history may have been higher than at present (and were certainly higher earlier than 3 Ga ago; e.g. Stöfler et al., 2006). Decreasing the diameter impactor considered from 1 km to 0.1 km increases the estimated number of impacts by about two orders of magnitude (Marchi et al., 2009), implying ~500 suitable locations on the lunar surface (although reducing the size of the impactor by a factor of ten reduces the mass of potential C- and N-rich resources by a factor of a thousand).

Finally, we reiterate that our estimates of the survival of C- and N-rich compounds is likely to be an underestimate because we have assumed that all such material is lost if the projectile fragments exceed their melting temperature (and if individual compounds transiently exceed their vaporisation temperatures). In reality, some of the material is likely to be retained locally to the impact site even for the higher velocity and impact angles considered here.

4.3. Detection of surviving CC meteoritic material

If, as we have argued, CC material may survive impact with the lunar surface, the next step will be to locate it. We have shown that highly oblique impacts (<15°) at low velocity (~5–10 km s^{-1}) maximise the potential for finding surviving C and N compounds in projectile fragments, so a survey of craters that show evidence for a highly oblique angle of impact would narrow down the number of potential areas to search. These craters would be elliptical, with crater rims elongated in the direction of impact and will likely exhibit secondary craters and scouring damage downrange from the impact site. Cratering experiments and numerical models have shown that the ellipticity of a crater increases dramatically with decreasing impact angle after impact angles fall below 15–20° (Bottke et al., 2000; Collins et al., 2011b; Elbeshausen et al., 2013; Michikami et al., 2017). Moreover, elliptical craters are more likely to form for low impact velocities (Michikami et al., 2017). Approximately 5% of lunar impact craters with diameters >1 km are designated as elliptical (Bottke et al., 2000), and these craters would, therefore, be the places to search for surviving CC material.

A start might be made in searching for low albedo material associated with elliptical craters. Dark patches associated with impact craters on the surface of asteroid 4 Vesta have been interpreted as surviving material from CC impactors (Reddy et al., 2012a, 2012b; McCord et al., 2012; De Sanctis et al., 2012; Prettyman et al., 2012). The detection of hydrated minerals in some of Vesta's dark material (De Sanctis et al., 2010, 2012; Russell et al., 2012; Palomba et al., 2014) lends further evidence to the idea that carbonaceous impactors have provided a projectile component to the Vestan regolith. Both experimental (Daly and Schultz, 2015) and modelling impact scenarios (Turrini et al., 2014, 2016) at typical Vestan impact velocities (<5 km s^{-1}) have shown that CC-like projectiles can survive and be retained within the regolith in proportions significant enough to explain dark material around impact craters on Vesta. It is true that average impact velocities on Vesta are significantly lower than those on the Moon (~5 km s^{-1} and ~15 km s^{-1}, respectively; O'Brien et al., 2011; Marchi et al., 2009), which will favour CC survival, but this is consistent with Vesta having many more dark impact-related splotches than the Moon. As discussed in Section 4.2 above, we already expect that surviving CC projectile material will be rare on the Moon, so the observational problem is to try to find it where it does occur.

Dark-haloed craters (DHCs) are common on the Moon (e.g., Salisbury et al., 1968; Kaydash et al., 2014; Kaur et al., 2015; Checketts et al., 2023), but these are mostly interpreted as pyroclastic volcanic deposits (Salisbury et al., 1968; Schultz and Spudis, 1983), differences in surface roughness or maturity (Kaydash et al., 2014), impact melt deposits (Hawke and Head, 1977; Bell and Hawke, 1984), or excavations of cryptomare (where dark basaltic material underlies higher albedo highland materials; e.g., Kaur et al., 2015; Checketts et al., 2023). To our knowledge, spectral analyses of lunar DHCs has yet to uncover any association with hydrated minerals, in contrast to those found on Vesta, but a determined search, especially in the vicinity of elliptical craters, may be worthwhile.

An additional method of detection could include a search for phyllosilicates, which are present in CCs, but are essentially non-existent in indigenous lunar materials (Joy et al., 2016). Analysing continuum slopes in near-infrared spectra has been used previously (Ostrowski et al., 2010) to identify and compare spectra of phyllosilicates on C-type asteroids to known phyllosilicates and CC samples and the same technique could be used for targeted areas on the Moon, concentrating in and around elliptical craters. The M^3 instrument on Chandrayaan-1 (Green et al., 2011) has provided a suitable dataset, although it mostly has a resolution of ~140 m $pixel^{-1}$ so it may only be suitable for identifying CC-rich fragments of the largest impactors. Finding evidence for surviving CC material after smaller impacts (e.g., closer to 100 m projectile diameters) would require a finer spatial resolution to identify smaller fragments. One possibility will be the High-resolution Volatiles and Minerals Moon Mapper (HVM^3) instrument on the forthcoming Lunar Trailblazer Mission (Ehlmann et al., 2022) which will have a resolution of 50–90 m $pixel^{-1}$ in the range 0.6–3.6 μm. The HVM^3 instrument will be complemented by the Lunar Thermal Mapper (LTM), a pushbroom, multichannel imaging thermal radiometer; LTM will have a spatial resolution of 40–70 m, capable of simultaneously mapping temperature (110–400 K), physical properties, and composition of water-bearing areas in HVM^3 pixels. These instruments may be able to detect hydrated clay minerals and associated features in smaller craters, detecting the remnants of survived carbonaceous chondrite material.

5. Conclusions

We have presented the results of impact simulations investigating the survival of CC material after impact with the lunar surface. In this case, survival is defined as material experiencing temperatures under a specific threshold, most importantly the material melt temperature (~2100 K). Additionally, survival of individual C- and N-bearing compounds after impact is deemed to occur if the maximum temperatures to which they are subjected is less than their vaporisation temperatures (Table 1). The only scenario in which significant amounts (16% of the original projectile mass) of nitrogen-bearing compounds survive is at the lowest impact velocity (5 km s^{-1}) and angle (15°). Impacts with velocities >10 km s^{-1} and angles >30° do not yield any significant amount of surviving solid material. Highly oblique impacts (≤15°) are expected to lead to concentrations of well-preserved projectile material downrange of the crater (Fig. 5). This material may be the most useful from a resource perspective, as it is likely to contain abundant C and N-bearing compounds within a small area away from the impact site. We have shown that as potential sources of C, and especially N, such impact sites compare favourably with polar PSRs.

Such low-velocity, oblique impacts are likely to have been rare on the Moon. We estimate that only ~5 CC-rich asteroids are likely to have hit the moon with velocities ≤10 km s^{-1} and impact angles ≤15° over the last 3 Ga (assuming the current lunar cratering rate). However, this is likely to be a conservative estimate because impact rates may have been higher earlier in Solar System history. If we consider smaller impactors, say 0.1 km rather than 1 km in diameter, the number of suitable impacts would be expected to be orders of magnitude higher (although each impact would yield a lower total mass of potential C- and N-rich resources).

We propose that a search for dark patches associated with elliptical impact craters, followed up with high-spatial resolution near-IR spectral

measurements, would be first step in prospecting for these potentially valuable resources on the lunar surface. Finally, we note that the expected small number of CC-rich deposits resulting from low-velocity oblique impacts provides another example of highly concentrated lunar resources (comparable in this respect to PSRs and the so-called 'peaks of eternal light'; Elvis et al., 2016), the management of which will benefit from international coordination if the risk of conflict between commercial and/or national operators engaged in their exploitation is to be avoided (e.g., Elvis et al., 2021; Crawford, 2021).

CRediT authorship contribution statement

Samuel H. Halim: Writing – original draft, Methodology, Investigation, Formal analysis, Conceptualization. **Ian A. Crawford:** Writing – review & editing, Supervision, Project administration, Methodology, Formal analysis, Conceptualization. **Gareth S. Collins:** Writing – review & editing, Supervision, Methodology, Investigation, Conceptualization. **Katherine H. Joy:** Writing – review & editing, Supervision, Investigation, Formal analysis. **Thomas M. Davison:** Writing – review & editing, Methodology, Investigation, Formal analysis.

Declaration of competing interest

The authors declare that they have no known competing financial interests or personal relationships that could have appeared to influence the work reported in this paper.

Data availability

Data will be made available on request.

Acknowledgements

We gratefully thank Boris Ivanov, Jay Melosh, Kai Wünnemann, Dirk Elbeshausen for their work in the development of iSALE. Samuel Halim would like to acknowledge STFC for funding through the award of a post-graduate studentship. KHJ acknowledges STFC (ST/V000675/1) and the Royal Society (URF\R\201009). KHJ and IAC acknowledge Leverhulme Trust (RPG-2019-222). GSC and TMD were funded by STFC Grant ST/S000615/1. The authors would like to acknowledge the UCL Kathleen High Performance Computing Facility (Kathleen@UCL) and associated support services in the completion of part of this work. IAC thanks Stephen Baxter for drawing his attention to the story by Haldeman (1981). We acknowledge our two referees, Meng-Hua Zhu and the other anonymous, for their thoughtful comments on our original manuscript that have improved it.

References

Alexander, C.M. O'd., Russell, S.S., Arden, J.W., Ash, R.D., Grady, M.M., Pillinger, C.T., 1998. The origin of chondritic macromolecular organic matter: a carbon and nitrogen isotope study. Meteoritics Planet Sci. 33, 603–622. https://doi.org/10.1111/j.1945-5100.1998.tb01667.x#.

Amsden, A., Ruppel, H., Hirt, C., 1980. SALE: a simplified ALE computer program for fluid flow at all speeds. LANL Rep. LA-8095.

Anand, M., Crawford, I.A., Balat-Pichelin, M., Abanades, S., van Westrenen, W., Péraudeau, G., Jaumann, R., Seboldt, W., 2012. A brief review of chemical and mineralogical resources on the Moon and likely initial in situ resource utilization (ISRU) applications. Planet. Space Sci. 74, 42–48.

Anderson, W.W., Ahrens, T.J., 1998. Shock wave equations of state of chondritic meteorites. AIP Conf. Proc. 429, 115. https://doi.org/10.1063/1.55475.

Avdellidou, C., Price, M., Delbo, M., Cole, M., 2016. Survival of the impactor during hypervelocity collisions – II. An analogue for high-porosity targets. MNRAS 464, 734–738. https://doi.org/10.1093/mnras/stw2381.

Basilevsky, A., Head, J., Horz, F., 2013. Survival times of meter-sized boulders on the surface of the Moon. Planet. Space Sci. 89, 118–126.

Basilevsky, A., Head, J., Horz, F., Ramsley, K., 2015. Survival times of meter-sized rock boulders on the surface of airless bodies. Planet. Space Sci. 117, 312–328.

Beech, M., Comte, M., Coulson, I., 2019. The production of terrestrial meteorites – moon accretion and lithopanspermia. Am. J. Astron. Astrophys. 7 (1), 1–9.

Bell, J.F., Hawke, B.R., 1984. Lunar dark-haloed impact craters: origin and implications for early mare volcanism. J. Geophys. Res. 89, 6899–6910.

Bland, P.A., Artemieva, N.A., Collins, G.S., Bottke, W.F., Bussey, D.B.J., Joy, K.H., 2008. Asteroids on the Moon: Projectile Survival during Low Velocity Impact, vol. 39. LPSC. Abstract #2045.

Bottke, W.F., Love, S.G., Tytell, D., Glotch, T., 2000. Interpreting the elliptical crater populations on Mars, Venus, and the moon. Icarus 145, 108–121. https://doi.org/10.1006/icar.1999.6323.

Bowling, T.J., Johnson, B.C., Marchi, S., De Sanctis, M.C., Castillo-Rogez, J.C., Raymond, C.A., 2020. An endogenic origin of cerean organics. Earth Planet Sci. Lett. 534, 116069.

Britt, D.T., Yeomans, D., Housen, K., Consolmagno, G., 2002. Asteroid density, porosity, and structure. In: Bottke, Jr.W.F., Cellino, A., Paolicchi, P., Binzel, R.P. (Eds.), Asteroids III. University of Arizona Press, Tucson, pp. 485–500.

Brookshaw, L., 1998. An equation of state for serpentine. Tech. Rep. Working Paper Series SC-MC-9813. Faculty of Sciences, University of Southern Queensland.

Brown, H.M., Boyd, A.K., Denevi, B.W., Henriksen, M.R., Manheim, M.R., Robinson, M. S., Speyerer, E.J., Wagner, R.V., 2022. Resource potential of lunar permanently shadowed regions. Icarus 377, 114874.

Bundy, F.P., 1989. Pressure-temperature phase diagram of elemental carbon. Phys. Stat. Mech. Appl. 156, 169–178. https://doi.org/10.1016/0378-4371(89)90115-5.

Burchell, M., Bowden, S., Cole, M., Price, M., Parnell, J., 2014a. Survival of organic materials in hypervelocity impacts of ice on sand, ice, and water in the laboratory. Astrobiology 14 (6), 473–485.

Burchell, M., McDermott, K., Price, M., Yolland, L., 2014b. Survival of fossils under extreme shocks induced by hypervelocity impacts. Phil. Trans. Royal Soc. A372, 20130190.

Burchell, M., Harriss, K., Price, M., Yolland, L., 2017. Survival of fossilised diatoms and forams in hypervelocity impacts with peak shock pressures in the 1–19 GPa range. Icarus 290, 81–88.

Cannon, K.M., 2021. Accessible carbon on the moon. https://doi.org/10.48550/arXiv.2104.13521.

Checketts, B.M., Hampton, I.L., Izquierdo, K., Sori, M.M., 2023. Global Mapping of Dark Halo Craters on the Moon. LPSC. Abstract #2045.

Chesley, S.R., Farnocchia, D., Nolan, M.C., Vokrouhlický, D., Chodas, P.W., Milani, A., Spoto, F., et al., 2014. Orbit and bulk density of the OSIRIS-REx target Asteroid (101955) Bennu. Icarus 235, 5–22. https://doi.org/10.1016/j.icarus.2014.02.020.

Christiansen, E., Cykowski, E., Ortega, J., 1993. Highly oblique impacts into thick and thin targets. Int. J. Impact Eng. 14, 157–168. https://doi.org/10.1016/0734-743x(93)90017-2.

Colaprete, A., et al., 2010. Detection of water in the LCROSS ejecta plume. Science 330, 463–468.

Collins, G.S., 2014. Numerical simulations of impact crater formation with dilatancy. J. Geophys. Res. 119, 2600–2619. https://doi.org/10.1002/2014JE004708.

Collins, G.S., Melosh, H.J., Wünnemann, K., 2011a. Improvements to the epsilon-alpha porous compaction model for simulating impacts into high-porosity solar system objects. Int. J. Impact Eng. 38, 434–439.

Collins, G.S., Elbeshausen, D., Davison, T.M., Robbins, S.J., Hynek, B.M., 2011b. The size-frequency distribution of elliptical impact craters. Earth Planet Sci. Lett. 310, 1–8. https://doi.org/10.1016/j.epsl.2011.07.023.

Consolmagno, G., Britt, D., Macke, R., 2008. The significance of meteorite density and porosity. Geochemistry 68, 1–29. https://doi.org/10.1016/j.chemer.2008.01.003.

Crawford, I.A., 2015. Lunar resources: a review. Prog. Phys. Geogr. 39, 137–167.

Crawford, I.A., 2021. Who speaks for humanity? The need for a single political voice. In: Chon Torres, O., Peters, T., Seckbach, J., Gordon, R. (Eds.), Astrobiology Ethics. Scrivener Publishing, Beverley, MA, USA, pp. 313–338.

Crawford, I.A., Baldwin, E., Taylor, E., Bailey, J., Tsembelis, K., 2008. On the survivability and detectability of terrestrial meteorites on the moon. Astrobiology 8, 242–252.

Crawford, I.A., Joy, K.H., 2014. Lunar exploration: opening a window into the history and evolution of the inner solar system. Phil. Trans. Royal Soc. A372, 20130315.

Crawford, I.A., et al., 2023. Lunar resources. Rev. Mineral. Geochem. 89, 829–868. https://doi.org/10.2138/rmg.2023.89.19.

Cronin, J.R., Moore, C.B., 1971. Amino acid analyses of the Murchison, Murray, and Allende carbonaceous chondrites. Science 172, 1327–1329, 10.1126.science.172.3990.1327.

Daly, R.T., Schultz, P.H., 2013. Experimental studies into the survival and state of the projectile. LPSC 44. Abstract #2240.

Daly, R.T., Schultz, P.H., 2015. Predictions for impactor contamination on Ceres based on hypervelocity impact experiments. Geophys. Res. Lett. 42 (19), 7890–7898.

Daly, R., Schultz, P., 2016. Delivering a projectile component to the Vestan regolith. Icarus 264, 9–19. https://doi.org/10.1016/j.icarus.2015.08.034.

Davison, T.M., Ciesla, F.J., Collins, G.S., Elbeshausen, D., 2014. The effect of impact obliquity on shock heating in planetesimal collisions. Meteorit. Planet. Sci. 49, 2252–2265. https://doi.org/10.1111/maps.12394.

Davison, T.M., Collins, G.S., Bland, P.A., 2016. Mesoscale modeling of impact compaction of primitive solar system solids. Astrophys. J. 821 (1), 68. https://doi.org/10.3847/0004-637x/821/1/68.

Davison, T.M., Collins, G.S., Elbeshausen, D., Wünnemann, K., Kearsley, A., 2011. Numerical modeling of oblique hypervelocity impacts on strong ductile targets. Meteorit. Planet. Sci. 46 (10), 1510–1524.

Day, J.M.D., Floss, C., Taylor, L.A., Anand, M., Patchen, A.D., 2006. Geochem. Cosmochim. Acta 70, 5957–5989. https://doi.org/10.2113/gselements.8.1.25.

De Sanctis, M.C., Coradini, A., Ammannito, E., Filacchione, G., Capria, M.T., Fonte, S., Magni, G., Barbis, A., Bini, A., Dami, M., Ficai-Veltroni, I., Preti, G., 2010. The VIR spectrometer. Space Sci. Rev. 163, 329–369, 10.1007s11214-010-9668-5.

De Sanctis, M.C., Combe, J.-P., Ammannito, E., Palomba, E., Longobardo, A., McCord, T. B., Marchi, S., Capaccioni, F., Capria, M.T., Mittlefehldt, D.W., Pieters, C.M., Sunshine, J., Tosi, F., Zambon, F., Carraro, F., Fonte, S., Frigeri, A., Magni, G., Raymond, C.A., Russell, C.T., 2012. Detection of widespread hydrated materials on Vesta by the VIR imaging spectrometer on-board the dawn mission. Astrophys. J. 758, L36. https://doi.org/10.1088/2041-8205/758/2/l36.

Ehlmann, B.L., Klima, R.L., Bennett, C.L., Blaney, D., Bowles, N., Calcutt, S., Dickson, J., Donaldson Hanna, K., Edwards, C.S., Green, R., House, M.A., Klesh, A., McCaa, C., Miura, J., Pieters, C., Seybold, C., Thompson, D., Williamson, W., Wood, J., 2022. Lunar trailblazer: a pioneering smallsat for lunar water and lunar geology. LPSC 53. Abstract# 2316.

Elbeshausen, D., Wünnemann, K., 2011. iSALE-3D: a three-dimensional, multi- material, multi-rheology hydrocode and its applications to large scale geodynamic processes. In: Proceedings of 11th Hypervelocity Impact Symposium 287±301.

Elbeshausen, D., Wünnemann, K., Collins, G.S., 2009. Scaling of oblique impacts in frictional targets: implications for crater size and formation mechanisms. Icarus 204, 716–731. https://doi.org/10.1016/j.icarus.2009.07.018.

Elbeshausen, D., Wünnemann, K., Collins, G.S., 2013. The transition from circular to elliptical impact craters. J. Geophys. Res. 118, 2295–2309. https://doi.org/10.1002/2013je004477.

Elvis, M., Milligan, T., Krolikowski, A., 2016. The peaks of eternal light: a near-term property issue on the Moon. Space Pol. 38, 30–38.

Elvis, M., Krolikowski, A., Milligan, T., 2021. Concentrated lunar resources: imminent implications for governance and justice. Phil. Trans. Royal Soc. A379, 20190563.

Fegley, B., Swindle, T.D., 1993. Lunar volatiles: implications for lunar resource utilization. In: Lewis, J., Matthews, M.S., Guerrieri, M.L. (Eds.), Resources of Near Earth Space. Tucson University Press, Tucson, AZ, USA, pp. 367–426.

Gault, D.E., Wedekind, J.A., 1978. Experimental studies of oblique impact. Proc. Lunar Planet Sci. Conf. 9, 3843–3875.

Goldstein, J.I., Henderson, E.P., Yakowitz, H., 1970. Investigation of lunar metal particles, 1970. In: Levinson, A.A. (Ed.), Geochimica et Cosmochimica Acta Supplement, Volume 1. Proceedings of the Apollo 11 Lunar Science Conference. New York: Pergammon Press, Houston, TX, pp. 499–512. Volume 1: Mineralogy and Petrology.

Green, R.O., Pieters, C., Mouroulis, P., Eastwood, M., Boardman, J., Glavich, T., Isaacson, P., Annadurai, M., Besse, S., Barr, D., Buratti, B., Cate, D., Chatterjee, A., Clark, R., Cheek, L., Combe, J., Dhingra, D., Essandoh, V., Geier, S., Goswami, J.N., 2011. The Moon Mineralogy Mapper (M3) imaging spectrometer for lunar science: instrument description, calibration, on-orbit measurements, science data calibration and on-orbit validation. J. Geophys. Res. 116 https://doi.org/10.1029/2011je003797.

Güldemeister, N., Wünnemann, K., Durr, N., Hiermaier, S., 2013. Propagation of impact-induced shock waves in porous sandstone using mesoscale modeling. Meteorit. Planet. Sci. 48, 115–133. https://doi.org/10.1111/j.1945-5100.2012.01430.x.

Haldeman, J., 1981. *Worlds*, Avon Books. New York (fiction).

Halim, S.H., 2023. Modelling the Survival of Meteoritic Material Exchanged between Planetary Bodies: Scientific and Commercial Implications. University of London. PhD Thesis. https://eprints.bbk.ac.uk/id/eprint/51489/.

Haskin, L.A., Colson, R.O., Vaniman, D.T., et al., 1993. A geochemical assessment of possible lunar ore formation. In: Lewis, J., Matthews, M.S., Guerrieri, M.L. (Eds.), Resources of Near Earth Space. Tucson University Press, Tucson, pp. 17–50.

Hawke, B.R., Head, J.W., 1977. Impact melt on lunar crater rims. In: Roddy, D.J., Pepin, R.B., Merrill, R.B. (Eds.), Impact and Explosion Cratering. Pergamon, New York, pp. 815–841.

Herbold, E.B., Owen, J.M., Swift, D.C., Miller, P.L., 2015. Simulations of defense strategies for Bennu: material characterization and impulse delivery. Procedia Eng. 173–180. https://doi.org/10.1016/j.proeng.2015.04.024.

Hurley, D.M., et al., 2023. Surface volatiles on the moon. Rev. Mineral. Geochem. 89, 787–828 et al. 2023.

Huss, G.R., Lewis, R.S., 1994. Noble gases in presolar diamonds I: three distinct components and their implications for diamond origins. Meteoritics 29, 791–810. https://doi.org/10.1111/j.1945-5100.1994.tb01094.x.

International Space Exploration Coordination Group (ISECG), 2020. Global Exploration Roadmap: Lunar Surface Exploration Scenario Update. National Aeronautics and Space Administration Headquarters, Washington, DC, 20546-0001. http://www.globalspaceexploration.org.

Ivanov, B.A., 2001. Mars/moon cratering rate ratio estimates. Space Sci. Rev. 96, 87–104. https://doi.org/10.1023/a:1011941121102.

Ivanov, B.A., Deniem, D., Neukum, G., 1997. Implementation of dynamic strength models into 2D hydrocodes: applications for atmospheric breakup and impact cratering. Int. J. Impact Eng. 20, 411–430.

Jolliff, B.L., Korotev, R.L., Haskin, L.A., 1993. An Iridium-Rich Iron Micrometeorite with Silicate Inclusions from the Moon. LPSC XXIV. Abstract #1366.

Joy, K.H., Zolensky, M.E., Nagashima, K., Huss, G.R., McKay, D.S., Ross, D.S., Kring, D. A., 2012. Direct detection of projectile relics from the end of the lunar basin–forming epoch. Science 336, 1426–1429. https://doi.org/10.1126/science.1219633.

Joy, K.H., Crawford, I.A., Curran, N., Zolensky, M., Fagan, A., Kring, D.A., 2016. The moon: an archive of small body migration in the solar system. Earth Moon Planets 118 (2–3), 133–158.

Joy, K.H., Tartèse, R., Messenger, S., Zolensky, M.E., Marrocchi, Y., Frank, D.R., Kring, D. A., 2020. The isotopic composition of volatiles in the unique Bench Crater carbonaceous chondrite impactor found in the Apollo 12 regolith. Earth Planet Sci. Lett. 540, 116265 https://doi.org/10.1016/j.epsl.2020.116265.

Jutzi, M., Benz, W., Michel, P., 2008. Numerical simulations of impacts involving porous bodies. Icarus 198 (1), 242–255. https://doi.org/10.1016/j.icarus.2008.06.013.

Kaur, P., Chauhan, P., Rajawat, A.S., Kumar, A.S.K., 2015. Study of olivine-rich dark halo crater – beaumont L in Mare Nectaris using high resolution remote sensing data. Planet. Space Sci. 109–110, 92–105. https://doi.org/10.1016/j.pss.2015.02.001.

Kaydash, V., Shkuratov, Y., Videen, G., 2014. Dark halos and rays of young lunar craters: a new insight into interpretation. Icarus 231, 22–33. https://doi.org/10.1016/j.icarus.2013.11.025.

Kring, D.A., Kramer, G.Y., Collins, G.S., Potter, R.W.K., Chandnani, M., 2016. Peak-ring structure and kinematics from a multi-disciplinary study of the Schrodinger impact basin. Nat. Commun. 7, 13161.

Kurosawa, K., Genda, H., 2018. Effects of friction and plastic deformation in shock-comminuted damaged rocks on impact heating. Geophys. Res. Lett. 45 (2), 620–626.

Lauretta, D.S., Bartels, A.E., Barucci, M.A., Bierhaus, E.B., Binzel, R.P., Bottke, W.F., Campins, H., et al., 2015. The OSIRIS-REx target asteroid (101955) Bennu: constraints on its physical, geological, and dynamical nature from astronomical observations. Meteorit. Planetary Sci. 50, 834–849. https://doi.org/10.1111/maps.12353.

Le Feuvre, M., Wieczorek, M.A., 2011. Nonuniform cratering of the Moon and a revised crater chronology of the inner Solar System. Icarus 214, 1–20. https://doi.org/10.1016/j.icarus.2011.03.010.

Liu, Y., Zhang, A., Taylor, L.A., 2009. Fragments of Asteroids in Lunar Rocks. 72nd Annual Meteoritical Society Meeting. Abstract #5434.

Marchi, S., Mottola, S., Cremonese, G., Massironi, M., Martellato, E., 2009. A new chronology for the Moon and Mercury. Astron. J. 137, 4936–4948. https://doi.org/10.1088/0004-6256/137/6/4936.

McCord, T.B., Li, J.-Y., Combe, J.-P., McSween, H.Y., Jaumann, R., Reddy, V., Tosi, F., Williams, D.A., Blewett, D.T., Turrini, D., Palomba, E., Pieters, C.M., De Sanctis, M. C., Ammannito, E., Capria, M.T., Le Corre, L., Longobardo, A., Nathues, A., Mittlefehldt, D.W., Schröder, S.E., 2012. Dark material on Vesta from the infall of carbonaceous volatile-rich material. Nature 491, 83–86. https://doi.org/10.1038/nature11561.

McCubbin, F.M., et al., 2023. Endogenous lunar volatiles. Rev. Mineral. Geochem. 89, 729–786.

Melosh, H.J., 1989. Impact Cratering: A Geologic Process. Oxford Univ., Clarendon, Oxford.

Melosh, H.J., 2007. A hydrocode equation of state for SiO_2. Meteorit. Planet. Sci. 42 (12), 2079–2098. https://doi.org/10.1111/j.1945-5100.2007.tb01009.x.

Melosh, H.J., Ryan, E.V., Asphaug, E., 1992. Dynamic fragmentation in impacts: hydrocode simulation of laboratory impacts. J. Geophys. Res. 97, 14735–14759.

Meyer, C., et al., 2011. Shock experiments in support of the Lithopanspermia theory: the influence of host rock composition, temperature, and shock pressure on the survival rate of endolithic and epilithic microorganisms. Meteorit. Planet. Sci. 46 (5), 701–718. https://doi.org/10.1111/j.1945-5100.2011.01184.x.

Michikami, T., Hagermann, A., Morota, T., Haruyama, J., Hasegawa, S., 2017. Oblique impact cratering experiments in brittle targets: implications for elliptical craters on the Moon. Planet. Space Sci. 135, 27–36. https://doi.org/10.1016/j.pss.2016.11.004.

Miljković, K., Collins, G.S., Patel, M.R., Chapman, D., Proud, W., 2012. High-velocity impacts in porous solar system materials. AIP Conf. Proc. 1426, 871–874.

Mimura, K., Toyama, S., 2005. Behavior of polycyclic aromatic hydrocarbons at impact shock: its implication for survival of organic materials delivered to the early Earth. Geochem. Cosmochim. Acta 69 (1), 201–209.

Mortimer, J., Verchovsky, A.B., Anand, M., 2016. Predominantly non-solar origin of nitrogen in lunar soils. Geochem. Cosmochim. Acta 193, 36–53.

Nagaoka, H., Takasawa, S., Nakamura, A., Sangen, K., 2013. Degree of impactor fragmentation under collision with a regolith surface-Laboratory impact experiments of rock projectiles. Meteorit. Planet. Sci. 49, 69–79. https://doi.org/10.1111/maps.12126.

National Institute for Occupational Safety and Health (NIOSH), 2019. Centers for disease control and prevention (CDC) - pocket guide to chem. Hazards: Silicon carbide. Available online: https://www.cdc.gov/niosh/npg/npgd0555.html.

Nishida, M., Hayashi, K., Toya, K., 2019. Influence of impact angle on size distribution of fragments in hypervelocity impacts. Int. J. Impact Eng. 128, 86–93. https://doi.org/10.1016/j.ijimpeng.2019.02.006.

O'Brien, D.P., Sykes, M.V., Tricarico, P., 2011. Collision probabilities and impact velocity distributions for Vesta and Ceres. LPSC 42. Abstract #2665.

O'Keefe, J.D., Ahrens, T.J., 1982. Cometary and meteorite swarm impact on planetary surfaces. J. Geophys. Res. 87, 6668–6680.

Ong, L., Asphaug, E., Korycansky, D., Coker, R., 2010. Volatile retention from cometary impacts on the Moon. Icarus 207 (2), 578–589.

Ostrowski, D.R., Gietzen, K., Lacy, C., Sears, D.W.G., 2010. An investigation of the presence and nature of phyllosilicates on the surfaces of C asteroids by an analysis of the continuum slopes in their near-infrared spectra. Meteorit. Planet. Sci. 45, 615–637. https://doi.org/10.1111/j.1945-5100.2010.01047.x.

Palomba, E., Longobardo, A., De Sanctis, M.C., Zambon, F., Tosi, F., Ammannito, E., Capaccioni, F., Frigeri, A., Capria, M.T., Cloutis, E.A., Jaumann, R., Combe, J.-P., Raymond, C.A., Russell, C.T., 2014. Composition and mineralogy of dark material units on Vesta. Icarus 240, 58–72. https://doi.org/10.1016/j.icarus.2014.04.040.

Parnell, J., et al., 2010. The preservation of fossil biomarkers during meteorite impact events: experimental evidence from biomarker-rich projectiles and target rocks. Meteorit. Planet. Sci. 45 (8), 1340–1358.

Pearson, V.K., Sephton, M.A., Franchi, I.A., Gibson, J.M., Gilmour, I., 2006. Carbon and nitrogen in carbonaceous chondrites: elemental abundances and stable isotopic compositions. Meteorit. Planet. Sci. 41, 1899–1918. https://doi.org/10.1111/j.1945-5100.2006.tb00459.x.

Pierazzo, E., Melosh, H.J., 2000. Hydrocode modeling of oblique impacts: the fate of the projectile. Meteorit. Planet. Sci. 35, 117–130. https://doi.org/10.1111/j.1945-5100.2000.tb01979.x.
Pierazzo, E., Chyba, C., 2002. Cometary delivery of biogenic elements to Europa. Icarus 157 (1), 120–127.
Pierazzo, E., Artemieva, N.A., Ivanov, B.A., 2005. Starting conditions for hydrothermal systems underneath Martian craters: hydrocode modeling. In: Kenkmann, T., Hörz, F., Deutsch, A. (Eds.), Large Meteorite Impacts III. Geological Society of America, Boulder, CO, pp. 443–457.
Pierazzo, E., et al., 2008. Validation of numerical codes for impact and explosion cratering: impacts on strengthless and metal targets. Meteorit. Planet. Sci. 43, 1917–1938.
Pierazzo, E., Vickery, A.M., Melosh, H.J., 1997. A reevaluation of impact melt production. Icarus 127 (2), 408–423.
Potter, R.W.K., 2012. Numerical modelling of basin-scale impact crater formation. Ph.D. thesis, Imperial College London.
Potter, R.W.K., Collins, G.S., 2013. Numerical modeling of asteroid survivability and possible scenarios for the Morokweng crater-forming impact. Meteorit. Planet. Sci. 48 (5), 744–757.
Prettyman, T.H., Mittlefehldt, D.W., Yamashita, N., Lawrence, D.J., Beck, A.W., Feldman, W.C., McCoy, T.J., McSween, H.Y., Toplis, M.J., Titus, T.N., Tricarico, P., Reedy, R.C., Hendricks, J.S., Forni, O., Le Corre, L., Li, J.-Y., Mizzon, H., Reddy, V., Raymond, C.A., Russell, C.T., 2012. Elemental mapping by dawn reveals exogenic H in Vesta's regolith. Science 338, 242–246, 10.1126sscience.1225354.
Prinetto, J., Colagrossi, A., Dottori, A., Troisi, I., Lavagna, M.R., 2023. Terrestrial demonstrator for a low-temperature carbothermal reduction process on lunar regolith simulant: design and AIV activities. Planet. Space Sci. 225, 105618.
Reddy, V., Nathues, A., Le Corre, L., Sierks, H., Li, J.-Y., Gaskell, R., McCoy, T., Beck, A. W., Schröder, S.E., Pieters, C.M., Becker, K.J., Buratti, B.J., Denevi, B., Blewett, D.T., Christensen, U., Gaffey, M.J., Gutierrez-Marques, P., Hicks, M., Keller, H.U., Maue, T., 2012a. Color and albedo heterogeneity of Vesta from dawn. Science 336, 700–704, 10.1126science.1219088.
Reddy, V., Le Corre, L., O'Brien, D.P., Nathues, A., Cloutis, E.A., Durda, D.D., Bottke, W. F., Bhatt, M.U., Nesvorny, D., Buczkowski, D., Scully, J.E.C., Palmer, E.M., Sierks, H., Mann, P.J., Becker, K.J., Beck, A.W., Mittlefehldt, D., Li, J.-Y., Gaskell, R., Russell, C. T., 2012b. Delivery of dark material to Vesta via carbonaceous chondritic impacts. Icarus 221, 544–559. https://doi.org/10.1016/j.icarus.2012.08.011.
Richardson, J.E., Melosh, H.J., Artemeiva, N.A., Pierazzo, E., 2005. Impact cratering theory and modeling for the deep impact mission: from mission planning to data analysis. Space Sci. Rev. 117, 241–267. https://doi.org/10.1007/s11214-005-3393-5.
Russell, S.S., Arden, J.W., Pillinger, C.T., 1996. A carbon and nitrogen isotope study of diamond from primitive chondrites. Meteorit. Planet. Sci. 31, 343–355. https://doi.org/10.1111/j.1945-5100.1996.tb02071.x.
Russell, C.T., Raymond, C.A., Coradini, A., McSween, H.Y., Zuber, M.T., Nathues, A., De Sanctis, M.C., Jaumann, R., Konopliv, A.S., Preusker, F., Asmar, S.W., Park, R.S., Gaskell, R., Keller, H.U., Mottola, S., Roatsch, T., Scully, J.E.C., Smith, D.E., Tricarico, P., Toplis, M.J., 2012. Dawn at Vesta: testing the protoplanetary paradigm. Science 336, 684–686, 10.1126science.1219381.
Salisbury, J.W., Adler, J.E.M., Smalley, V.G., Ring, J., 1968. Dark-haloed craters on the moon. MNRAS 138, 245–249. https://doi.org/10.1093/mnras/138.2.245.
Schultz, P.H., Spudis, P.D., 1983. Beginning and end of lunar mare volcanism. Nature 302, 233–236. https://doi.org/10.1038/302233a0.
Sephton, M.A., 2002. Organic compounds in carbonaceous meteorites. Nat. Prod. Rep. 19, 292–311. https://doi.org/10.1039/b103775g.
Shoemaker, E.M., 1962. Interpretation of lunar craters. In: Kopal, A. (Ed.), Physics and Astronomy of the Moon. Academic Press, New York, pp. 283–351.
Shoemaker, E.M., Wolfe, R.F., Shoemaker, C.S., 1990. In: Sharpton, V.L., Ward, P.D. (Eds.), Geological Society of America Special Paper 247, Global Catastrophes in Earth History: an Interdisciplinary Conference on Impacts, Volcanism, and Mass Mortality, vol. 155.
Stöfler, D., Ryder, G., Ivanov, B.A., Artemieva, N.A., Cintala, M.J., Grieve, R.A.F., 2006. Cratering history and lunar chronology. Res. Min. Geochem. 60, 519–596.
Sugita, S., Honda, R., Morota, T., Kameda, S., Sawada, H., Tatsumi, E., Yamada, M., et al., 2019. The geomorphology, color, and thermal properties of Ryugu: implications for parent-body processes. Science 364. https://doi.org/10.1126/science.aaw0422.
Svetsov, V., Shuvalov, V., 2015. Water delivery to the Moon by asteroidal and cometary impacts. Planet. Space Sci. 117, 444–452.
Thompson, S.L., Lauson, H.S., 1972. Improvements in the Chart-D Radiation Hydrodynamic Code III: Revised Analytical Equation of State: Sandia Laboratories Report SC-RR-71 0714, p. 119.
Turrini, D., Combe, J.P., McCord, T.B., et al., 2014. The contamination of the surface of Vesta by impacts and the delivery of the dark material. Icarus 240, 86–102. https://doi.org/10.1016/j.icarus.2014.02.021.
Turrini, D., Svetsov, V., Consolmagno, G., Sirono, S., Pirani, S., 2016. Olivine on Vesta as exogenous contaminants brought by impacts: constraints from modeling Vesta's collisional history and from impact simulations. Icarus 280, 328–339. https://doi.org/10.1016/j.icarus.2016.07.009.
Veverka, J., Thomas, P., Harch, A., et al., 1999. NEAR encounter with asteroid 253 mathilde: overview. Icarus 140, 3–16. https://doi.org/10.1006/icar.1999.6120.
Wakita, S., Genda, H., 2019. Fates of hydrous materials during planetesimal collisions. Icarus 328, 58–68. https://doi.org/10.1016/j.icarus.2019.03.008.
Wamelink, G.W.W., Frissel, J.Y., Krijnen, W.H.J., Verwoert, M.R., Goedhart, P.W., 2014. Can plants grow on mars and the moon: a growth experiment on mars and moon soil simulants. PLoS One 9, e103138. https://doi.org/10.1371/journal.pone.0103138.
Weiss, I.M., Muth, C., Drumm, R., Kirchner, H.O.K., 2018. Thermal decomposition of the amino acids glycine, cysteine, aspartic acid, asparagine, glutamic acid, glutamine, arginine and histidine. BMC Biophys. 11, 10.1186.s13628-018-0042-4.
Wells, L., Armstrong, J., Gonzalez, G., 2003. Reseeding of early earth by impacts of returning ejecta during the late heavy bombardment. Icarus 162 (1), 38–46.
Wickham-Eade, J., 2017. Fragmentation of Carbon-Bearing Projectiles and the Effects on Their Raman Spectra Due to Hypervelocity Impacts. University of Kent, Kent, England. Ph. D. Thesis.
Wickham-Eade, J., Burchell, M., Price, M., Harriss, K., 2018. Hypervelocity impact fragmentation of basalt and shale projectiles. Icarus 311, 52–68.
Wieczorek, M., Weiss, B., Stewart, S., 2012. An impactor origin for lunar magnetic anomalies. Science 335, 1212–1215. https://doi.org/10.1126/science.1214773.
Wieczorek, M.A., Neumann, G.A., Nimmo, F., Kiefer, W.S., Taylor, G.J., Melosh, H.J., Phillips, R.J., Solomon, S.C., Andrews-Hanna, J.C., Asmar, S.W., Konopliv, A.S., Lemoine, F.G., Smith, D.E., Watkins, M.M., Williams, J.G., Zuber, M.T., 2013. The crust of the moon as seen by GRAIL. Science 339, 671–675, 10.1126science.1231530.
Wingo, D., 2004. Moonrush: Improving Life on Earth with the Moon's Resources. Apogee Books, Burlington.
Wood, J.A., Marvin, U.B., Reed, J.B., Taylor, G.J., Bower, J.F., Powell, B.N., Dickey, J.S., 1971. Mineralogy and petrology of the Apollo 12 lunar sample. Smithsonian Astrophys. Obs. Spec. Rep. 333, 177.
Wünnemann, K., Collins, G.S., Melosh, H., 2006. A strain-based porosity model for use in hydrocode simulations of impacts and implications for transient crater growth in porous targets. Icarus 180, 514–527. https://doi.org/10.1016/j.icarus.2005.10.013.
Wünnemann, K., Collins, G.S., Osinski, G., 2008. Numerical modelling of impact melt production in porous rocks. Earth Planet Sci. Lett. 269 (3–4), 530–539.
Yang, Y., et al., 2022. Impact remnants rich in carbonaceous chondrites detected on the Moon by the Chang'e-4 rover. Nat. Astron. 6, 207–213.
Yue, Z., Johnson, B., Minton, D., Melosh, H., Di, K., Hu, W., Liu, Y., 2013. Projectile remnants in central peaks of lunar impact craters. Nat. Geosci. 6 (6), 435–437.
Zolensky, M.E., Weisberg, M.K., Buchanan, P.C., Mittlefehldt, D.W., 1996. Mineralogy of carbonaceous chondrite clasts in HED achondrites and the Moon. Meteorit. Planet. Sci. 31, 518–537.